HHS Public Access

Author manuscript

Nat Neurosci. Author manuscript; available in PMC 2018 August 20.

Published in final edited form as:

Nat Neurosci. 2018 March ; 21(3): 329–340. doi:10.1038/s41593-018-0083-7.

Microglia-mediated recovery from ALS-relevant motor neuron degeneration in a mouse model of TDP-43 proteinopathy

Krista J. Spiller[1,*], **Clark R. Restrepo**[1], **Tahiyana Khan**[1], **Myrna A. Dominique**[1], **Terry C. Fang**[2], **Rebecca G. Canter**[2], **Christopher Roberts**[2], **Kelly R. Miller**[1], **Richard M. Ransohoff**[3], **John Q. Trojanowski**[1], and **Virginia M-Y. Lee**[1]

[1]Center for Neurodegenerative Disease Research (CNDR), Institute on Aging, Department of Pathology and Laboratory Medicine, Perelman School of Medicine, University of Pennsylvania, Philadelphia, PA, USA

[2]Biogen, 225 Binney Street, Cambridge, MA, USA

[3]Third Rock Ventures, Boston, MA

Abstract

Though motor neurons (MNs) selectively degenerate in amyotrophic lateral sclerosis (ALS), other cell types are likely involved in this disease. We recently generated rNLS8 mice in which human TDP-43 (hTDP-43) pathology could be reversibly induced in neurons and expected microglia would contribute to neurodegeneration. However, only subtle microglial changes were detected during disease in the spinal cord, despite progressive MN loss, but microglia still reacted to inflammatory triggers in these mice. Notably, after the hTDP-43 expression was suppressed, microglia dramatically proliferated and changed their morphology and gene expression profiles. These abundant, reactive microglia selectively cleared neuronal hTDP-43. Finally, when microgliosis was blocked during the early recovery phase using PLX3397, a CSF1R/c-kit inhibitor, rNLS8 mice failed to regain full motor function, revealing an important neuroprotective role for microglia. Therefore, reactive microglia exert neuroprotective functions in this ALS model and definition of the underlying mechanism could point towards novel therapeutic strategies.

Reactive microglia have been hypothesized to increase the severity of several neurodegenerative disorders [1], but recently there is a growing appreciation that the nature of the microglial reaction to CNS pathology is not uniform and is contingent on the timing and diversity of microglial subtypes involved. Further, emerging data reveal fundamental roles for microglia in maintaining homeostasis[2], including controlling the formation of synapses [3], refining neuronal circuits, eliminating redundant synapses [4], and facilitating neurotrophin-

[*]Corresponding Author; spillerk@upenn.edu.

Contributions:

K.J.S., R.M.R, and V.M.-Y.L. designed research; K.J.S., C.R.R., T.K, K.R.M, M.A.D., T.C. F, R.G.C. performed research; K.J.S., T.K., M.A.D., T.C. F, R.G.C., C.R., and C.R.R. analyzed data; K.J.S., J.Q.T., R.M.R. and V.M.-Y.L. wrote the paper.

Competing financial interests:

T.C.F., R.G.C., and C.R. are employees and stockholders of Biogen, Inc.

mediated healing responses to injury [5]. Currently, both microglial-mediated neurotoxicity and neuroprotection in disease are active areas of research.

Microglia have been specifically implicated in ALS. For example CD68+ microglia were found to be dispersed in degenerating white matter of postmortem sporadic ALS (sALS) spinal cord (SC), though much less extensively in the ventral horns [6]. Clinically, PET radiotracers showed increased glial activation in motor and extra-motor cerebral regions in small groups of ALS patients during the disease progression [7–9]. Additionally, several studies have measured alterations in cytokines in cerebrospinal fluid from ALS patients during disease [10, 11]. However, studies which examined gene expression changes in SC samples from sALS patients did not find changes in microglia-specific genes or pathways [12, 13].

The majority of research on the role of microglia in ALS comes from studies in the most commonly used model of familial ALS, mSOD1 mice, in which mSOD1 in microglia was shown to contribute to the disease progression[1415, 16].When microglial proliferation or function was blocked, there was an amelioration of the disease in mSOD1 mice [17, 18]. Given that SOD1 is a ubiquitously expressed protein that is normally secreted by microglia under physiological conditions, has been shown to be neuroprotective[19], and that most ALS patients (~97%) do not have mutations in this gene, it is important to examine neuroinflammation in patients without SOD1 mutations, as well as in a mouse model that may be more relevant to the majority of ALS cases.

Since >90% of ALS patients have an accumulation of cytoplasmic TDP-43 aggregates in postmortem SC [20] and aberrant forms of TDP-43 have been implicated in MN death [21, 22], we propose that investigating non-cell autonomous changes in the SC in response to pathological TDP-43 may be more disease relevant. Some studies have shown that TDP-43 is associated with increased levels of neuroinflammatory markers[23–25], but it has been difficult to assess the direct effects of TDP-43 aggregates on microglia activation *in vivo*. We therefore used our new inducible mouse model of ALS, rNLS8 mice[26], to examine the relationship between TDP-43, disease onset/progression, and neuroinflammation. rNLS8 mice express *hTDP43ΔNLS* in neurons in a doxycycline (DOX)-dependent manner, such that *hTDP43ΔNLS* expression is suppressed in the presence of DOX [26], allowing us to induce the formation of TDP-43 aggregates and measure microglial responses . Moreover, we have previously shown that when we halt disease by suppressing *hTDP43ΔNLS*, pathological TDP-43 is cleared, MN loss ceases, and the surviving MNs innervate vacated neuromuscular junctions (NMJs)[26, 27]. Thus, we can also use this model to examine the relationship between these regenerative events and changes in microglia.

Results

Only subtle microglial changes are detected during disease onset/progression in rNLS8 SC

Our previous studies characterized the disease course in rNLS8 mice following induction of *hTDP43ΔNLS* in the primary affected cells, neurons[26] (Fig. 1a). Next, we characterized changes in microglia from rNLS8 mice before and during disease. We confirmed that

hTDP-43 is not expressed in microglia in rNLS8 mice upon DOX removal (Supplementary Fig. 1), such that any changes we observe reflect a response to chronic neuronal *hTDP43ΔNLS* expression rather than a direct impact on microglia themselves. Unexpectedly, we found only slight changes in microglia density in the SC and no changes in microglial morphology during the disease course (key time-points shown in Fig. 1b–g), even after 8 weeks of expression when significant MN death has occurred and the remaining MNs have cytoplasmic accumulations of hTDP-43 and nuclear clearance of endogenous TDP-43 (Fig. 1d,g and Supplementary Fig. 1). Quantification of IBA-1$^+$ cells per mm^2 or % area occupied by CD68 further confirmed that there was only a ~10% increase in the number of microglia at lumbar level SCs of rNLS8 mice at 6 weeks off DOX compared to rNLS8 mice on DOX and no change in CD68 at 2, 4, or 6 weeks off DOX (Fig. 1h–i).

To test the ability of these glia to respond to canonical inflammatory stimuli, we either performed a unilateral sciatic nerve crush or injected lipopolysaccharide (LPS, i.p.) in rNLS8 mice at 2 weeks off DOX, when neurons exhibit full transgene expression (Supplementary Fig. 2). In both experimental paradigms, microglia mount a typical response to the stimulus. Thus, the absence of reactive microgliosis in the SC during disease in rNLS8 mice does not arise from a globally suppressed microglial phenotype.

Postmortem lumbar SC samples from sALS patients have less reactive microglia than patients with a *SOD1* mutation

Since our finding that microgliosis is not a major feature of the disease course in the SC of rNLS8 mice differs from previous findings in mSOD1 mice, we examined postmortem SC tissues from ALS patients to address the relevance of these disparate results for the human disease. We immunostained lumbar SCs from 5 control patients, 10 patients with clinically probable or definite sALS, 6 ALS patients with a *C9orf72* mutation, and 4 patients with mutations in *SOD1* with IBA-1 to assess reactive microgliosis and NeuN to measure MN loss (Fig. 2). We observed dramatically different levels of reactive microgliosis in the grey matter of ALS ventral horns, depending on whether the patient had a *SOD1* mutation or not (Fig. 2e). There was variability in scores between individual sALS cases, possibly reflecting different, as-yet-unidentified etiologies of disease in these patients. However, 50% of sALS cases had microglia levels equal or less than control patients and only 2 sALS patients had microgliosis scores in the same range as samples from patients with mutant *SOD1* (Supplementary Table 1).

Taken together, patients with a *SOD1* mutation had an average inflammation score that was significantly higher than those of sALS patients, patients with a *C9orf72* mutation, and controls: 2.6 ± 0.5 vs. 1.2 ± 1.1 vs. 1.0 ± 0.8 vs. 0.9 ±0.5. Interestingly, of the 4 patients with identified *SOD1* mutations, one did not have clinical symptoms at her time of death (76 years old) nor did she show any postmortem evidence of ALS or any other neurodegenerative abnormalities. We further confirmed that this patient did not have any MN loss specifically in the lumbar SC (Fig. 2c). However, the grey matter surrounding those MNs contained an abundance of reactive microglia, suggesting that mutant SOD1-bearing microglia may have important differences in reactivity, independent of neuronal death. We also observed slightly increased IBA-1 reactivity in *mSOD1*, but not sALS, patients in other

brain regions that are not typically associated with ALS (Supplementary Fig. 3). Therefore, the low levels of microgliosis observed in late stage disease rNLS8 mice (Fig. 1d) is similar to the SC inflammation in many of the terminal sALS samples from our brain bank.

In early disease recovery, there is a robust increase in reactive microglia

When *hTDP43ΔNLS* is suppressed after chronic expression, there is a dramatic increase in microglial number and a change in their morphology concurrent with hTDP-43 clearance from neurons in the rNLS8 SC (Fig. 3). The peak number of microglia in the ventral horn occurs after 1 week of transgene suppression, or "early recovery" (Fig. 3b and g), where we detected 157 ± 7.0 IBA-1^{+} cells/mm^{2} in ventral horns of rNLS8 mice. This is significantly more than at 6 weeks off DOX (92.8± 5.4 microglia/mm^{2}) and in control rNLS8 SC (82.9 ± 3.0 microglia/mm^{2}). By 8 weeks back on DOX, when hTDP-43 is completely cleared from SC neurons (Fig. 3c) and motor symptoms have resolved[27], microglia return to basal levels, with a ramified phenotype. This process takes place as MN loss is halted (Fig. 3d–f), with approximately 14 MNs/ventral horn after 6 weeks of DOX removal and reintroduction. Further, during early recovery, the microglia have a reactive morphology, with significantly larger cell bodies (Fig. 3h) and shorter, thicker processes (Fig. 3h–i). Therefore, in early recovery, the number of SC microglia rapidly increases and morphology changes from ramified to reactive.

To test if these distinct microglial changes in early recovery relied on prior neuron death, we suppressed *hTDP43ΔNLS* after only 2 weeks of expression, a time when hTDP-43 is expressed at high levels in the brain and SC[26], but before we detect significant MN death in the lumbar SC[27, 28] (Fig. 4a–c). Remarkably, we found a dramatic increase in the number of reactive microglia (Fig. 4c) in these rNLS8 mice at the 2 weeks off DOX + 1 week back on time-point, compared to littermates that were on or off DOX continuously for the whole 3 weeks (Fig. 4a,b). We also evaluated motor pools outside of the SC that are resistant to pathological TDP-43 triggered cell death[27]. We found the same pattern of microglial activation after transgene suppression in both the trigeminal nucleus (Fig. 4d–e) and facial nucleus (Fig. 4f–g), further confirming that this microglial response does not rely on cell death.

We also observed this microglial reaction during recovery in brain regions besides the SC (Supplementary Fig. 4), but this response was not as dramatic relative to disease, probably reflecting intrinsic regional diversity in microglial responses. Further, to explore whether the suppression of *hTDP43ΔNLS* induces a restricted proliferation of microglia or a global inflammatory response with astrocytosis, we immunostained rNLS8 SCs at various time-points with GFAP (Supplementary Fig. 4), and found that there was no obvious increase in astrocytosis at any time-point. We also did not find significant changes in expression of genes associated with the reactive astrocyte phenotype[29] by qPCR in RNA isolated from whole lysate of rNLS8 SC before, during, or after disease (Supplementary Fig. 4).

To investigate if microglial activation during transgene suppression is a general feature of DOX-inducible mice or is specific to tissues in which full-length pathological TDP-43 is being cleared, we examined a different bigenic line of mice with NEFH-controlled, DOX-inducible expression of a TDP-43 C-terminal fragment (amino acids 208–414, designated

"208")[30] during chronic transgene expression and after 1 week recovery (Fig. 4h–j). Unlike rNLS8 mice, these NEFH-208 mice do not exhibit MN loss or develop gross motor dysfunction, and the 208 TDP-43 C-terminal fragments do not induce nuclear TDP-43 clearance or form large cytoplasmic inclusions (Supplementary Fig. 5). We found no difference in microglia counts in the lumbar SC of NEFH-208 mice that were continuously off DOX versus 1 week recovery (88 ± 3.7 vs. 90.6 ± 3.3 microglia/ mm^2, Fig. 4j), which is in stark contrast to the ~70 % increase that we see with suppression of the mutant full-length TDP-43 in the rNLS8 line.

The increased microgliosis results from central proliferation and not infiltration of peripheral myeloid cells

To determine if the source of the increased microgliosis during early recovery in rNLS8 mice is entirely due to local proliferation or is accompanied by peripheral infiltration, we performed 2 separate experiments: one that involved labeling peripheral circulating myeloid cells and the other based on depleting them and assessing whether the microglial response was attenuated. First, whole body irradiated rNLS8 mice were rescued with bone-marrow cells from Actin-GFP mice so that their peripheral immune system was reconstituted by GFP-tagged donor-derived cells. Two months later, chimeric mice were separated into 3 groups: 1) control- rNLS8 mice maintained on DOX; 2) disease- rNLS8 mice off DOX for 4 weeks; and 3) recovery- rNLS8 mice off DOX for 6 weeks followed by 1 week on DOX (Fig. 5a). We confirmed that the peripheral immune system was successfully reconstituted with GFP^+ cells by immunostaining the spleen (Fig. 5b) and liver, and using flow cytometry to identify $CD11B^+/GFP^+$ cells in blood. The microglial response pattern was unchanged in chimeric rNLS8 mice, with little microglia activation during disease and a sharp increase during recovery. In all groups, the microglia were GFP^-, suggesting that the increased number of IBA-1^+ cells during early recovery did not include infiltrated cells (Fig. 5c).

Clodronate-filled liposomes trigger apoptosis in myeloid cells[31], and so were used to dramatically reduce peripheral macrophage populations, but not resident microglia, in rNLS8 mice during early recovery (Fig. 5d–f; Supplementary Fig. 6). This depletion had no effect on microgliosis during early recovery in rNLS8 mice (Fig. 5g–k), in which both PBS- and clodronate-liposome treated animals had the same marked increase in reactive microglia in the SC (139 ± 16 vs. 137 ± 22 IBA-1^+ cells/mm^2). Further, CD44 has recently been identified as a marker for infiltrating immune populations[32], and we found that the microglia in the rNLS8 SC during recovery were CD44 negative (Fig. 5l).

Finally, to document rapid proliferation of resident microglia following *hTDP43ΔNLS* suppression, 6 week off DOX or early recovery rNLS8 mice were injected daily for 1 week with 5-bromodeoxycytidine (BrdU, 50 mg/kg, i.p.). Early-recovery rNLS8 mice had ~12 $BrdU^+/$IBA-1^+ cells per ventral horn, compared to only ~2 $BrdU^+$ microglia per ventral horn in rNLS8 mice at 7 weeks off DOX (Supplementary Fig. 7). Taken together, these 3 experiments indicate that microgliosis after transgene suppression arises from the proliferative response of resident microglia, not invasion from the periphery.

Transcriptomic profiling of microglia isolated from rNLS8 mice reveals unique disease and recovery associated changes

Total RNA was extracted from CD11b^{+}CD45^{lo} microglia from SCs of rNLS8 mice during early and intermediate disease time-points (2 and 6 weeks off DOX, n=7 and 8), early recovery (6 weeks off + 1 week back on DOX, n=9), and control mice (rNLS8 mice maintained on DOX and DOX-matched nTg mice, n=14 total) for sequencing to determine disease and recovery-relevant gene expression changes in these cells (Supplementary Fig. 8). The microglia cell lineage was confirmed by gene expression of microglial genes (e.g., *Cx3cr1, Irf8*), but low/absent markers for astrocytes (*Gfap*) and neurons (*Nefh*) (Supplementary Fig. 8). Principal component analysis (PCA) and unsupervised hierarchical clustering revealed some overlap between different disease samples, with the early disease and control samples being particularly intermingled, and variability in the late disease replicates (Supplementary Fig. 8). However, late disease and recovery signals could be clearly distinguished when directly compared (Fig. 6a).

Despite only observing a 10 % increase in the number of SC microglia and no obvious change in their morphology at 6 weeks off DOX (Fig. 1), we found 465 genes that were changed over 1.5 fold at that time-point relative to control (Fig. 6b, Supplementary Fig. 9). Of the genes that were upregulated, many were part of pathways associated with the production of inflammatory molecules (e.g., *Hmgb1* and *Trem1* signaling pathways; Supplementary Fig. 9).

Previous microglia profiling studies in mSOD1 and other mouse models of neurodegeneration have identified transcriptional signatures associated with long-term disease[33–35], and we next wanted to compare these with the gene expression changes in rNLS8 microglia. First, Chiu and colleagues hypothesized that mSOD1 microglia express both neurotoxic and neuroprotective factors[33]. We thought these phenotypes might be more differentiated in our samples during late disease and early recovery, but instead found that many of the identified putative “neurotoxic” genes were similarly upregulated in both sets of samples (e.g., *Mmp12* and *Cybb*, Supplementary Fig. 10). Further, Krasemann and colleagues identified homeostatic genes that were downregulated in neurodegeneration such as *Tgfb1, Jun*, and *Mef2a*, but none of these were consistently changed across our samples (Supplementary Fig. 10). However, the genes that they found to be upregulated (e.g., *Apoe, Itgax, Spp1*) were also upregulated in rNLS8 microglia taken from both late disease and early recovery[34]. Finally, Keren-Shaul et al. identified genes that were upregulated in microglia during neurodegenerative disease progression (such as *Lpl, Ctsb,* and *Ctsd*), which they called DAM[35]. Again, these genes were upregulated similarly in both late disease and recovery in rNLS8 microglia (Supplementary Fig. 10). These findings suggest that those gene sets are in fact associated with disease, but not exclusively.

When *hTDP43ΔNLS* is suppressed for 1 week, 171 of the genes that are up in late disease are downregulated (Fig 6c). Many of these genes were related to changes in RNA processing, including those involved in mRNA splicing (*Clasrp, Pabpn1, Ccnl2*), RNA binding (*Cirbp*), and protein transcription (*Gabpb2*), and “alternative splicing” was an identified suppressed gene ontology pathway. This result is intriguing, given the importance

of normally functioning nuclear TDP-43 for proper RNA-processing[36], and the down-regulation of endogenous mouse TDP-43 after chronic expression of *hTDP43ΔNLS*[26].

Further, compared to control samples, 125 genes are upregulated over 1.5 fold in recovery (Fig. 6d–e), and 76 of these genes were uniquely upregulated when compared to changed genes during late disease (Fig. 6d, Supplementary Fig. 10). These genes comprise several interesting pathways including cell adhesion molecules and phagosome (DAVID), and antigen presentation (Ingenuity Pathway Analysis). These gene changes fit well with observations that microglia often directly contact neurons following transgene suppression, with some surviving neurons being nearly completely surrounded by reactive microglia (Fig. 6f). This apparent contact and the upregulated genes associated with phagosome formation next led us to consider whether these microglial functions might account for hTDP-43 clearance after transgene suppression (Fig. 7).

Microglia clear neuronal hTDP-43, and this is selective over other cytosolic neuronal proteins

Given the gene expression signatures and the increase in microglial expression of CD68 (Fig. 5i–j, Supplementary Fig. 11), we next asked whether microglia might be active participants in the clearance of hTDP-43 from neuronal cytoplasm. Following transgene suppression, we found that microglia that were not surrounding neurons contained hTDP-43 and expressed CD68 (Fig. 7a; Supplementary Fig. 11). In contrast, microglia at 6 weeks off DOX rarely contained hTDP-43 (Fig. 7b), with an average of 28.5 IBA-1+ cells containing hTDP-43 at 1 week recovery, compared to ~4 at 6 weeks off DOX (48.7 ± 2.2 % of all ventral horn microglia vs. 10.2 ± 3.3%). If non-viable neurons were nonspecifically releasing their contents or if microglia were engulfing dead cells, we reasoned that other cytoplasmic neuronal proteins would also be detected in the microglia during early recovery, but found that other neuron specific proteins were rarely within microglia (Supplementary Fig. 12). This suggests that hTDP-43 is being selectively cleared by microglia, though we cannot rule out the possibility that the other neuronal proteins may just be under the detection limit of immunofluorescence. The means by which hTDP-43 is taken up by microglia during recovery remains uncertain, but selective release of hTDP-43 from neurons could precede its uptake by microglia.

We next overexpressed another protein in rNLS8 SC MNs to exclude the trivial possibility that the differential proportion of hTDP-43-bearing microglia resulted from hTDP-43 being overexpressed. Newborn rNLS8 mice were injected with AAV9.GFP (i.c.v) to tag MNs with GFP (Supplementary Fig. 13). When these mice reached adulthood, we removed DOX for 6 weeks, followed by 3 days or 1 week back on DOX (Fig. 7c–h). GFP levels remained high in SC MNs, but absent from microglia during recovery in AAV.GFP-injected rNLS8 mice (Fig. 7e–f). In contrast, the majority of these microglia contained hTDP-43, suggesting that the uptake of neuronal hTDP-43 is very selective over other cytosolic proteins, even when they are overexpressed (Fig. 7g–h).

Microglia are necessary for motor recovery after *hTDP43ΔNLS* suppression in rNLS8 mice

To elucidate the functional role that microgliosis plays during the recovery phase in rNLS8 mice, we used a CSF1R/c-kit inhibitor, PLX3397[37], to assess the consequence of microglia suppression on motor recovery. rNLS8 mice were taken off DOX for 4 weeks and then subsequently given DOX for 2 weeks. For the last 3 weeks of this timeline, rNLS8 mice received Nutella in a petri dish at the bottom of their cage daily (n=5) or the same amount of Nutella, but with PLX3397 mixed in at 1000 mg/kg (n=5, Fig. 8a). The motor symptoms in rNLS8 mice given Nutella only were largely resolved after 2 weeks of transgene suppression (Fig. 8c). However, all of the rNLS8 mice that were treated with PLX3397 still displayed hindlimb clasping and some maintained a hunched posture (Fig. 8b–c). Further, compound muscle action potentials (CMAPs) recorded from gastrocnemius trended lower in PLX3397-treated mice compared to controls (Fig. 8d). PLX3397 significantly blocked the increased microgliosis at 2 weeks recovery in all tested rNLS8 mice, even depleting microglia levels below that of nTg mice in 3 of the 5 mice (Fig. 8e). We speculate that the variability in the amount of microglia reduction stemmed from differences in Nutella consumption, despite all mice having equal access. There were no apparent differences between the two groups in the number of SC astrocytes.

We next analyzed the consequence of microglia depletion on clearance of hTDP-43. hTDP-43 was still strongly detected by immunofluorescence in the PLX3397-treated rNLS8 mice, but not in controls (Fig. 8f–h). Ventral horn hTDP-43 levels varied inversely to microglia density, suggesting that microglia are needed for clearing the intracellular pathological TDP-43 (Supplementary Table 2), and consistent with the possibility that the mechanism of clearance requires microglial-neuronal contact. Importantly, we confirmed by qPCR that *hTDP43ΔNLS* was suppressed in all rNLS8 mice after 2 weeks of DOX reintroduction, regardless of treatment group (Supplementary Fig. 14).

We also found that control rNLS8 mice had 14 % more intact NMJs in the tibialis anterior (TA) than PLX3397 treated mice, suggesting that axonal dieback continued in the microglia-depleted animals despite transgene suppression (Fig. 8i). rNLS8 SCs also have significantly fewer MNs after microglial reduction (Fig. 8j–l). However, the remaining microglia in PLX3397-treated SCs still appear to be functional, as they express CD68 (Fig. 8m–n) LPL, and Trem2 (Supplementary Fig. 14). Moreover, the relationship between the amounts of microglial depletion varied tightly with the effect on recovery parameters. Animals with the fewest microglia following PLX3397 treatment had the lowest CMAPs, the fewest remaining lumbar MNs, the most TA denervation, and the least clearance of hTDP-43 from SC neurons (Supplementary Table 2). This was not an effect of the drug itself as the same administration regime did not affect the neuromuscular system of nTg controls (Supplementary Fig. 14). Therefore, reducing microglia by 35–90% in rNLS8 mice dramatically altered recovery after transgene suppression.

Discussion

Our results show that microglia are critically involved in recovery from a sALS-like neurodegenerative disease in the SC that is linked to mislocalization and aggregation of TDP-43 in the rNLS8 mouse model. When TDP-43 triggered MN disease processes are

halted, there is a dramatic increase in reactive microglia concurrent with hTDP-43 clearance and functional motor recovery. When this increased microgliosis is blocked, rNLS8 mice fail to make a full recovery over the course of 2 weeks. The full spectrum of microglial activities associated with recovery remains to be determined, although the active, contact-dependent clearance of pathological TDP-43 from neurons is likely to play a central role.

In mouse models involving peripheral nerve transection, microglia have been shown to become activated, surround injured MNs, and displace synapses in a process dubbed "synaptic stripping", all of which precedes regeneration[38, 39]. Given that we see a similar pattern of microgliosis in rNLS8 mice after transgene suppression, prior to the MNs expanding their innervation field and beginning to express proteins that they typically do not express[27], it is intriguing to speculate that microglia may contribute to this plasticity. Furthermore, there are compelling studies over the last 5 years showing that microglia can be active participants in circuit refinement and pruning processes[40]. Debris clearance by microglia declines with aging and is associated with an inadequate regenerative response[41]. We previously showed that aged rNLS8 mice had a diminished recovery relative to young mice[28], and we now propose that microglial senescence may be a contributing factor.

Further, we also showed that microgliosis arises as a result of a proliferative response from resident CNS microglia (Fig. 5). But what cues launch this proliferation and why aren't these signal(s) deployed during the disease process? We know that it is not simply an effect of DOX on mice, because neither NEFH8-208 nor nTg mice show changes in microgliosis in response to DOX being removed or added to their diet (Fig. 4j). Moreover, the signal for proliferation cannot simply lie downstream of the accumulation of pathological TDP-43, because these accumulations are very abundant throughout the disease course in the SC, and yet microglia levels remain stable. Other questions of interest are: would pathological hTDP-43 be transmitted to other neurons and seed further TDP-43 aggregation if the microglia were not available to eliminate it? Perhaps of greatest translational relevance, if we could selectively induce the relevant microglia functions during disease, would the progression of ALS be arrested? Finally, it has been demonstrated that microglia in different brain regions have intrinsic baseline differences in gene expression and sensitivity[42–44], so fully exploring microglial responses to disease and recovery in other brain regions will be an interesting future direction.

Our results are markedly different from previous findings in studies of other mouse models of ALS. For example, studies in the mSOD1 mouse model showed that eliminating microglia is beneficial[18]. We think the critical difference between these mice and our rNLS8 mice is that the rNLS8 mice have WT microglia and an intact blood-brain barrier (Supplementary Fig. 6). Nevertheless, those studies in mSOD1 mice generated great excitement in the use of anti-inflammatory drugs to treat ALS patients, but no such drugs have successfully been translated to therapeutic success in ALS patients. In this study, when we looked at postmortem SC tissue in the areas immediately surrounding MNs in 25 individuals, we found that most sALS patients only showed occasional increased microgliosis relative to controls, but all patients harboring *SOD1* mutations showed extensive microgliosis (Fig. 2). This suggests that rNLS8 mice may be a more translatable model for the vast majority of sALS patients, with respect to microglial inflammation.

Altogether, our study shows that microglia in the environment of MNs can have a positive impact on their survival and ultimately in their recovery from disease. We found that genes associated with cellular contact and phagosome formation are uniquely upregulated in microglia during recovery, which may mediate their protective interactions with surviving MNs. Though there are currently no clinical strategies available to effectively target TDP-43 in patients, this research suggests that doing that in combination with encouraging appropriate microgliosis could be a valuable therapeutic direction. Further, using this inducible transgene system to activate microgliosis allows us to model microglia proliferation for repair separately from proliferation in response to nerve injury itself.

Finally, researchers have previously called for the targeting and reduction of microglial cells in order to slow ALS disease progression[45]. We now propose the opposite strategy; that is, findings ways to encourage appropriate microglia-mediated inflammation during the onset/progression of ALS to clear pathological TDP-43 proteins and boost axonal regeneration. Understanding the impact of normally functioning microglia on TDP-43 clearance and axonal outgrowth can provide new therapeutic strategies for patients even in late disease stages.

Online Methods

Tg and nTg mice

As described previously[26], rNLS8 mice were generated by crossing new Tg lines overexpressing tetracycline transactivator (tTA) protein under the control of the human *NEFH* promoter with an existing Tg line that can be induced with DOX manipulation to express human TDP-43 with a defective nuclear localization signal (hTDP-43ΔNLS). Bigenic 208 TDP-43 Tg mice were produced by crossing *tetO*-208 TDP-43 Tg mice with the *NEFH*-tTA Tg mice. For both lines, a DOX diet (Dox Diet #3888, Bio-Serv) inhibits tTA from binding to the tetracycline promoter element, repressing hTDP-43 expression. When mice are taken off DOX and given standard chow (Rodent Diet 20 #5053, PicoLab), hTDP-43 expression is activated. For all studies, male and female mice were used and mice were between 2 and 5 months old when DOX was initially removed from their diets. Randomization was not possible for group selection when comparing rNLS8 mice to controls, because the animals needed to be genotyped. However, after genotyping, rNLS8 mice were randomly assigned to different DOX treatment conditions and/or drug treatment. Experimenters were blinded to the genotype/treatment of each mouse during data collection and identities were decoded later for analysis, using identification numbering based on toe tattooing. Sample sizes were chosen based on prior publications using these mice[26–28]. All procedures were performed in accordance with the NIH Guide for the Care and Use of Experimental Animals. Studies were approved by the Institutional Animal Care and Use Committee of the University of Pennsylvania.

Nerve crush

The lateral thigh of rNLS8 or nTg mice (n=4 each, 2 weeks off DOX) was shaved, and a 0.5–1 cm incision in the skin was made over the lateral femur. The sciatic nerve was

localized and crushed with a hemostat for 15 seconds. The skin incision was closed with silk sutures and the animals were allowed to recover on a warming blanket.

LPS injections

rNLS8 mice that were 2 weeks off DOX (n=6) or nTg (n=3) were injected with LPS at 4 mg/kg (i.p.) at a volume of 10 mL/kg and perfused 6 or 18 hours later and their SCs were prepared for immunostaining, as described below.

Irradiation experiments

Adult rNLS8 mice received whole body lethal irradiation using 950rad (9.5 Gy) gamma irradiation delivered for 10 minutes. 1 to 2 hours after irradiation, mice received a bone marrow transplantation of approximately 5×10^6 cells administered in a total volume of 200 μL via tail vein injection using a 30 gauge needle. Animals were allowed to fully recover from the procedure for 8 weeks. After recovery, in 2 of the 3 groups of animals (Fig. 5a), DOX treatment was stopped in order to initiate disease processes, including those that were allowed to progress in the disease state for 4 weeks prior to sacrifice and those that were placed back on DOX chow after 6 weeks of disease in order to allow for a recovery phase.

BrdU treatment

rNLS8 mice that were 6 weeks off DOX were either reintroduced to DOX (n=4) or kept on the standard diet (n=4). These animals were injected daily with BrdU (Sigma-Aldrich) at 50 mg/kg (i.p.) for 6 days and were perfused 24 hours after the last injection to assess the presence of newborn cells in the spleen and lumbar SC in early recovery or during disease.

Injection of Liposomes

Clodronate- and PBS-loaded liposomes were purchased from Lipsoma. The suspension of liposome encapsulated clodronate is ca. 5 mg of clodronate per 1 ml of the suspension. nTg (n=6) or rNLS8 mice off DOX (n=7) were injected with clodronate liposomes or PBS liposomes (10 mL/kg, i.p.) 3 days before DOX was reintroduced to the animals' chow and continued for an additional 7 days while the animals recovered on DOX. This protocol was based on discussions through the Web site www.ClodronateLiposomes.org.

PLX3397 treatment

PLX3397 (1Click Chemistry) mixed into Nutella at 1000 mg/kg, or Nutella only, was added to polysterene culture dishes, placed at the bottom of cages housing nTg or rNLS8 mice, and changed every 24 hours for 3 weeks. We found Nutella to be a suitable vehicle for voluntary oral ingestion, and chose it as a less stressful alternative to gavage. Each animal ate between 0.5–1.25 g Nutella over the course of the 24 hours, in addition to 2–3 grams of regular or DOX chow (Fig. 8a).

Experiments with viral vectors

AAV9.CMV.PI.eGFP.WPRE.bGH (3.3×10^{13} GC/mL, Penn Vector Core) was thawed on ice and the virus solution was colored by addition of a small amount of Fast Green dye (Sigma-Aldrich, St. Louis, MI). For i.c.v. injections, P1 pups were anesthetized by hypothermia and,

using a 31 gauge 1/2 cc insulin syringe (BD Ultra-Fine* II Short Needle Insulin Syringe, VWR), 2 μL of virus was injected into the third ventricle. Successful injection was confirmed by bilateral spread. If the dye did not spread to both ventricles, the injections were deemed unsuccessful and the pups were sacrificed. Remaining pups were returned to their mother and health was monitored to adulthood.

Muscle physiology

To perform the CMAP recordings, mice were anesthetized and their hind legs were shaved. The sciatic nerve was stimulated through bipolar needle electrodes by injecting brief electrical currents (0.3 Hz, 0.5 ms pulse duration, starting at 0 and incrementally increasing by 5 mA). The response from the gastrocnemius was recorded using needle electrodes placed in the center of the muscle and in the tendon. The M-wave was measured at each escalating amplitude, until the maximal response was elicited and did not increase further. Maximum evoked amplitudes were analyzed using pClamp 10 software (Molecular Devices).

Preparation of mouse lysates and qPCR

Mice were perfused with phosphate buffered saline (PBS), and a fast dissection was performed to remove cortex and SC. Mouse tissue samples were homogenized in QIAzol lysis buffer (Qiagen), chloroform was added and they were spun down at 12000 rpm 4C for 15min. RNA was isolated using miRNeasy Kit (Qiagen). Quality and concentration were tested using NanoDrop 2000. RNA was then reverse transcribed to cDNA using the SuperScript III (Invitrogen). Quantitative polymerase chain reaction (qPCR) was performed on the cDNA using SYBR Green PCR Master Mix (Life Technologies) and the following primers for hTDP-43: CCTAATTCTAAGCAAAGCCAAGATG and ACAGCGCCCCACAAACA, for Emp1: GAGACACTGGCCAGAAAAGC and TAAAAGGCAAGGGAATGCAC, for Serping1: ACAGCCCCCTCTGAATTCTT and GGATGCTCTCCAAGTTGCTC, and for Fkbp5: GGCAAACTCTAGGAGGCTTAAA and CTTACAGCTCCCACCAGAATAC. The qPCR plate was read using Applied Biosystems 7500 Fast Real Time PCR system. Gene expression was measured relative to *Actb* (β-actin). 3 technical replicates were run for each sample.

Immuofluorescence and quantification

rNLS8 mice, 208 TDP-43 Tg mice, and nTg controls were perfused with ice-cold PBS followed by 10 % formalin and then the brain, lumbar SC, spleen, liver, and hindlimb muscles were surgically removed. Peripheral tissues were washed in PBS overnight, and the CNS tissue was post-fixed in 10 % formalin overnight. All were then washed in PBS and then processed in a sucrose gradient up to 30% for cryoprotective embedding.

To analyze MN populations in the brainstem and lumbar SC, tissues were sectioned at 20 μm and immunostained using the following primary antibodies: guinea pig anti-VAChT (1:1,000, CNDR), rabbit anti-VAChT (1:5000, CNDR), mouse anti-human TDP-43 monoclonal antibody (MAb) (0.06 μg/mL, CNDR, clone 5104), rat anti-CD68 (1:200, Bio-rad), rat anti-Cd11b (1:200, Bio-rad), rabbit or goat anti-IBA-1 (1:1000, Wako and Novus), goat anti-CHAT (1:500, Millipore), mouse anti-NeuN (1:5000, Millipore), sheep anti-Trem2

(1:500, R&D Systems), rabbit anti-CD44 (1:100, Millipore), mouse anti-LPL (1:50, Abcam), rabbit anti-GFAP (1:5000, Dako), and rat anti-BrdU (1:1000, Bio-rad).

After overnight incubation with primaries, sections were washed and then incubated with Alexa Fluor secondary antibodies (1:1000, Molecular Probes). Tissues were either imaged using a Nikon Eclipse Ni inverted microscope or a Leica TCS SPE. For the confocal imaging of microglia, 10 *z*-steps spaced 1–3 μm apart were collected per image and a maximum projection was created for each.

For the quantification of MN numbers, MNs were counted in transverse 20 μm cryosections, 100 μm apart, over the length of 1 mm. For quantification and morphological analysis of microglia, IBA-1 and DAPI co-positive cells were counted in the ventral horn grey matter only over the length of L3-L5, using Image J and NIS-Elements software.

For spleen and liver, sections were cut longitudinally at 10 μm and immunostained with rat anti-F4/80 (1:200, Bio-rad) and IBA-1.

The TA muscle was sectioned at 30 μm longitudinally, and immunostained with VAChT to label nerve terminals and α-bungarotoxin conjugated to Alexa-488 (BTX, 1:1000) to label motor endplates. The percentage of NMJ innervation was determined by dividing the total number of areas of overlap between VAChT and BTX signals (total number innervated endplates) by the number of areas of BTX signal (total number of endplates) on consecutive longitudinal 30 μm cryosections of muscles. We observed 400–1000 NMJs per TA.

Microglial isolation

Mice were euthanized with ketamine/xylazine cocktail and perfused with ice-cold PBS. SCs were flushed from the spinal column using PBS and placed in ice-cold HBSS with HEPES. Tissue was homogenized using Wheaton (Millville, NJ, USA) tissue grinders to achieve a single cell suspension. The homogenate was centrifuged through a 30% Percoll (GE Healthcare) gradient to remove myelin and enrich for microglia. After washing with FACS buffer (HBSS, HEPES, BSA, EDTA) cells were Fc-blocked (CD16/32, Cat. #101321, Biolegend, San Diego, CA, USA) and stained with CD11b-PE (Cat. #553311, BD Biosciences, MA, USA) and CD45-BV421 (Cat #103134, Biolegend). DRAQ7 was used for dead cell exclusion. Cells were sorted on an ARIA Fusion Flow Cytometer and collected directly into RNA lysis buffer (Buffer RLT, Qiagen, Hilden, Germany). A portion of cells were sorted into FACS buffer to assess purity. DRAQ5 was used to mark all nucleated cells post sort. Purity was greater than >90%.

RNA processing

RNA was isolated with the RNeasy Micro Kit Plus (Qiagen). RNA quality was assessed on the 2100 Bioanalyzer with the RNA 6000 Nano Kit (Agilent, Santa Clara, CA, USA) and quantified using Quant-iT RiboGreen (Life Technologies, Carlsbad, CA, USA). Libraries were constructed using the SMART-Seq Ultra Low-input (Clontech, Mountain View, CA, USA) and NexteraXT kits (Illumina, San Diego, CA, USA). Libraries were sequenced at an average depth of 20 million paired end reads.

Transcriptomic data analysis

After sequencing, FASTQ files were generated by clustering BCL files to paired FASTQ files with a BCL2FASTQ pipeline in line with standard Illumina sequence generation. RNA-Seq analysis was performed in the commercial platform Omicsoft Arraystudio, including raw RNA-Seq data quality control, filtering and trimming of reads, and alignment to the mouse genome (mm10 assembly, with gene annotations from Gencode release M6 and Ensembl81) using the Omicsoft OSA4 aligner[46]. Greater than 30 million paired-end fragments were generated from each RNA sample analyzed, with the percentages of uniquely and non-uniquely mapped paired end reads ranging from 89 to 92% and 3 to 5%, respectively, which was consistent with high quality RNA-Seq data. Gene-level quantification of aligned reads was performed in Omicsoft using a module adopted from RSEM[47], and differential gene expression was performed using an Omicsoft implementation of DESeq2[48]. Plots were generated in the OmicSoft interface and using BioVenn[49]. Pathway insights were obtained using the Ingenuity Pathway Analysis (IPA) software from Qiagen.

Human study

Detailed clinical characteristics (disease duration, age at death, site of onset, etc.) were ascertained from an integrated autopsy database at CNDR. Genotyping for a *C9orf72* repeat expansion or the coding regions of other genes associated with ALS/FTLD-TDP (SOD1, TARDBP, UBQLN2) were performed as previously reported[50]. Sample sizes were based on availability of patient material, which was donated and autopsied at the Center for Neurodegenerative Disease Research (University of Pennsylvania) between 2008 and 2016. Patient details can be found in Supplementary Table 1. Written informed consent for autopsy and analysis of tissue sample data was obtained for all patients, either from the patients themselves or their next of kin. Samples were obtained with ethics committee approval.

For the analysis of microglial pathology, lumbar section of 6 or 20 μm thickness were cut from paraffin-embedded specimens. For IHC, all slides were deparaffinized and rehydrated in a series of xylene and graded ethanol. Microwave antigen retrieval was performed with Vector Antigen Unmasking Solution at 1:100 dilution in dH_2O for 15 minutes at 95°C. After cooling, slides were washed in 0.1 M Tris buffer (pH 7.6) and blocked in 0.1 M Tris/2% FBS. Sections were stained using polyclonal rabbit anti-Iba1 antibody (1:1000, Wako Chemicals) and mouse anti-NeuN (1:1000, Millipore) and incubated overnight at 4°C. Sections were then rinsed and washed in Tris, blocked in 0.1 M Tris/2% FBS, and then incubated with Alexa Fluor secondary antibodies (1:1000, Molecular Probes) for 2 hours. After incubation with secondary antibodies, sections were washed and briefly immersed in 0.3% Sudan Black in 70% Ethanol to reduce background autofluorescence. The extent of microglial activation of the ventral horn grey matter was rated on a 4-point ordinal scale (0, none; 1, mild; 2, moderate; 3, severe/numerous) by three independent investigators and these scores were averaged.

Statistics and Reproducibility

All experiments described in this paper were performed once, using 3–8 independent animals per group as defined in figure legends. At least 10 sections of SC were imaged per animal (sampled over the length of 1 mm), yielding at least 20 10X images per animal. No

data points were excluded from analysis in any experiment, although the TA of one animal was not analyzed in the PLX3397 treatment study due to experimenter error during tissue sectioning. Data were checked for normality using the Shapiro-Wilk method and equal variance by the Brown-Forsythe method. Statistical significance was determined using unpaired or paired two tail t-tests when comparing two groups and one-way ANOVA when comparing multiple groups, using SigmaPlot. For significant results by one-way ANOVA, all pairwise multiple comparisons were made using the Holm-Sidak method. A *p*-value of less than 0.05 was considered significant.

Data availability and Accession Code

Further information on experimental design is available in the Life Sciences Reporting Summary. Additional data supporting the findings of this study are available from the corresponding author upon request. The GEO accession number for the RNA-Seq data is GSE109171.

Supplementary Material

Refer to Web version on PubMed Central for supplementary material.

Acknowledgments

The authors wish to thank S. Leight for administrative support, K.L. Spiller and K. Brunden for valuable feedback, V. Van Deerlin and E. Suh for the genetic analysis of the ALS patients studied here, E. Lee for help with microscopy, as well as D. Cotton-Samuel for assistance with tissue sectioning and immunostaining. This work was supported by the Judith and Jean Pape Adams Charitable Foundation and the ALS Association (K.J.S.), AG PO1-017586 (V.M.-Y.L.) as well as gifts from the Koller and Pottruck families. Finally, we thank our ALS patients and their families for making human ALS tissue samples available to us for our studies.

References

1. Block ML, Zecca L, Hong JS. Microglia-mediated neurotoxicity: uncovering the molecular mechanisms. Nature reviews. Neuroscience. 2007; 8:57–69. [PubMed: 17180163]
2. Waisman A, Ginhoux F, Greter M, Bruttger J. Homeostasis of Microglia in the Adult Brain: Review of Novel Microglia Depletion Systems. Trends in immunology. 2015; 36:625–636. [PubMed: 26431940]
3. Hong S, Dissing-Olesen L, Stevens B. New insights on the role of microglia in synaptic pruning in health and disease. Current opinion in neurobiology. 2016; 36:128–134. [PubMed: 26745839]
4. Paolicelli RC, et al. Synaptic pruning by microglia is necessary for normal brain development. Science. 2011; 333:1456–1458. [PubMed: 21778362]
5. Dougherty KD, Dreyfus CF, Black IB. Brain-derived neurotrophic factor in astrocytes, oligodendrocytes, and microglia/macrophages after spinal cord injury. Neurobiology of disease. 2000; 7:574–585. [PubMed: 11114257]
6. Henkel JS, et al. Presence of dendritic cells, MCP-1, and activated microglia/macrophages in amyotrophic lateral sclerosis spinal cord tissue. Annals of neurology. 2004; 55:221–235. [PubMed: 14755726]
7. Turner MR, et al. Evidence of widespread cerebral microglial activation in amyotrophic lateral sclerosis: an [11C](R)-PK11195 positron emission tomography study. Neurobiology of disease. 2004; 15:601–609. [PubMed: 15056468]
8. Alshikho MJ, et al. Glial activation colocalizes with structural abnormalities in amyotrophic lateral sclerosis. Neurology. 2016; 87:2554–2561. [PubMed: 27837005]

9. Zurcher NR, et al. Increased in vivo glial activation in patients with amyotrophic lateral sclerosis: assessed with [(11)C]-PBR28. NeuroImage. Clinical. 2015; 7:409–414. [PubMed: 25685708]
10. Tateishi T, et al. CSF chemokine alterations related to the clinical course of amyotrophic lateral sclerosis. Journal of neuroimmunology. 2010; 222:76–81. [PubMed: 20381883]
11. Martinez HR, et al. Altered CSF cytokine network in amyotrophic lateral sclerosis patients: A pathway-based statistical analysis. Cytokine. 2017; 90:1–5. [PubMed: 27741429]
12. Rabin SJ, et al. Sporadic ALS has compartment-specific aberrant exon splicing and altered cell-matrix adhesion biology. Human molecular genetics. 2010; 19:313–328. [PubMed: 19864493]
13. Offen D, et al. Spinal cord mRNA profile in patients with ALS: comparison with transgenic mice expressing the human SOD-1 mutant. Journal of molecular neuroscience : MN. 2009; 38:85–93. [PubMed: 18651250]
14. Clement AM, et al. Wild-type nonneuronal cells extend survival of SOD1 mutant motor neurons in ALS mice. Science. 2003; 302:113–117. [PubMed: 14526083]
15. Boillee S, et al. Onset and progression in inherited ALS determined by motor neurons and microglia. Science. 2006; 312:1389–1392. [PubMed: 16741123]
16. Beers DR, et al. Wild-type microglia extend survival in PU.1 knockout mice with familial amyotrophic lateral sclerosis. Proceedings of the National Academy of Sciences of the United States of America. 2006; 103:16021–16026. [PubMed: 17043238]
17. Martinez-Muriana A, et al. CSF1R blockade slows the progression of amyotrophic lateral sclerosis by reducing microgliosis and invasion of macrophages into peripheral nerves. Scientific reports. 2016; 6:25663. [PubMed: 27174644]
18. Frakes AE, et al. Microglia induce motor neuron death via the classical NF-kappaB pathway in amyotrophic lateral sclerosis. Neuron. 2014; 81:1009–1023. [PubMed: 24607225]
19. Polazzi E, et al. Copper-zinc superoxide dismutase (SOD1) is released by microglial cells and confers neuroprotection against 6-OHDA neurotoxicity. Neuro-Signals. 2013; 21:112–128. [PubMed: 22572742]
20. Neumann M, et al. Ubiquitinated TDP-43 in frontotemporal lobar degeneration and amyotrophic lateral sclerosis. Science. 2006; 314:130–133. [PubMed: 17023659]
21. Kabashi E, et al. Gain and loss of function of ALS-related mutations of TARDBP (TDP-43) cause motor deficits in vivo. Human molecular genetics. 2010; 19:671–683. [PubMed: 19959528]
22. Wegorzewska I, Bell S, Cairns NJ, Miller TM, Baloh RH. TDP-43 mutant transgenic mice develop features of ALS and frontotemporal lobar degeneration. Proceedings of the National Academy of Sciences of the United States of America. 2009; 106:18809–18814. [PubMed: 19833869]
23. Herman AM, Khandelwal PJ, Rebeck GW, Moussa CE. Wild type TDP-43 induces neuro-inflammation and alters APP metabolism in lentiviral gene transfer models. Exp Neurol. 2012; 235:297–305. [PubMed: 22402344]
24. Swarup V, et al. Deregulation of TDP-43 in amyotrophic lateral sclerosis triggers nuclear factor kappaB-mediated pathogenic pathways. The Journal of experimental medicine. 2011; 208:2429–2447. [PubMed: 22084410]
25. Tong J, et al. Expression of ALS-linked TDP-43 mutant in astrocytes causes non-cell-autonomous motor neuron death in rats. The EMBO journal. 2013; 32:1917–1926. [PubMed: 23714777]
26. Walker AK, et al. Functional recovery in new mouse models of ALS/FTLD after clearance of pathological cytoplasmic TDP-43. Acta neuropathologica. 2015; 130:643–660. [PubMed: 26197969]
27. Spiller KJ, et al. Selective Motor Neuron Resistance and Recovery in a New Inducible Mouse Model of TDP-43 Proteinopathy. The Journal of neuroscience : the official journal of the Society for Neuroscience. 2016; 36:7707–7717. [PubMed: 27445147]
28. Spiller KJ, et al. Progression of motor neuron disease is accelerated and the ability to recover is compromised with advanced age in rNLS8 mice. Acta neuropathologica communications. 2016; 4:105. [PubMed: 27687289]
29. Liddelow SA, et al. Neurotoxic reactive astrocytes are induced by activated microglia. Nature. 2017; 541:481–487. [PubMed: 28099414]

30. Walker AK, et al. An insoluble frontotemporal lobar degeneration-associated TDP-43 C-terminal fragment causes neurodegeneration and hippocampus pathology in transgenic mice. Human molecular genetics. 2015; 24:7241–7254. [PubMed: 26476406]
31. van Rooijen N, Sanders A, van den Berg TK. Apoptosis of macrophages induced by liposome-mediated intracellular delivery of clodronate and propamidine. Journal of immunological methods. 1996; 193:93–99. [PubMed: 8690935]
32. Korin B, et al. High-dimensional, single-cell characterization of the brain's immune compartment. Nature neuroscience. 2017; 20:1300–1309. [PubMed: 28758994]
33. Chiu IM, et al. A neurodegeneration-specific gene-expression signature of acutely isolated microglia from an amyotrophic lateral sclerosis mouse model. Cell reports. 2013; 4:385–401. [PubMed: 23850290]
34. Krasemann S, et al. The TREM2-APOE Pathway Drives the Transcriptional Phenotype of Dysfunctional Microglia in Neurodegenerative Diseases. Immunity. 2017; 47:566–581. e569. [PubMed: 28930663]
35. Keren-Shaul H, et al. A Unique Microglia Type Associated with Restricting Development of Alzheimer's Disease. Cell. 2017; 169:1276–1290. e1217. [PubMed: 28602351]
36. Buratti E, Baralle FE. Multiple roles of TDP-43 in gene expression, splicing regulation, and human disease. Frontiers in bioscience : a journal and virtual library. 2008; 13:867–878. [PubMed: 17981595]
37. Elmore MR, et al. Colony-stimulating factor 1 receptor signaling is necessary for microglia viability, unmasking a microglia progenitor cell in the adult brain. Neuron. 2014; 82:380–397. [PubMed: 24742461]
38. Wake H, Moorhouse AJ, Miyamoto A, Nabekura J. Microglia: actively surveying and shaping neuronal circuit structure and function. Trends in neurosciences. 2013; 36:209–217. [PubMed: 23260014]
39. Graeber MB, et al. The microglia/macrophage response in the neonatal rat facial nucleus following axotomy. Brain research. 1998; 813:241–253. [PubMed: 9838143]
40. Schafer DP, Stevens B. Phagocytic glial cells: sculpting synaptic circuits in the developing nervous system. Current opinion in neurobiology. 2013; 23:1034–1040. [PubMed: 24157239]
41. Damani MR, et al. Age-related alterations in the dynamic behavior of microglia. Aging cell. 2011; 10:263–276. [PubMed: 21108733]
42. Grabert K, et al. Microglial brain region-dependent diversity and selective regional sensitivities to aging. Nature neuroscience. 2016; 19:504–516. [PubMed: 26780511]
43. De Biase LM, et al. Local Cues Establish and Maintain Region-Specific Phenotypes of Basal Ganglia Microglia. Neuron. 2017; 95:341–356. e346. [PubMed: 28689984]
44. Tay TL, et al. A new fate mapping system reveals context-dependent random or clonal expansion of microglia. Nature neuroscience. 2017; 20:793–803. [PubMed: 28414331]
45. Barbeito AG, Mesci P, Boillee S. Motor neuron-immune interactions: the vicious circle of ALS. Journal of neural transmission. 2010; 117:981–1000. [PubMed: 20552235]
46. Hu J, Ge H, Newman M, Liu K. OSA: a fast and accurate alignment tool for RNA-Seq. Bioinformatics. 2012; 28:1933–1934. DOI: 10.1093/bioinformatics/bts294 [PubMed: 22592379]
47. Li B, Dewey CN. RSEM: accurate transcript quantification from RNA-Seq data with or without a reference genome. BMC bioinformatics. 2011; 12:323. [PubMed: 21816040]
48. Love MI, Huber W, Anders S. Moderated estimation of fold change and dispersion for RNA-seq data with DESeq2. Genome biology. 2014; 15:550. [PubMed: 25516281]
49. Hulsen T, de Vlieg J, Alkema W. BioVenn - a web application for the comparison and visualization of biological lists using area-proportional Venn diagrams. BMC genomics. 9:488. [PubMed: 18925949]
50. Brettschneider J, et al. TDP-43 pathology and neuronal loss in amyotrophic lateral sclerosis spinal cord. Acta neuropathologica. 2014; 128:423–437. [PubMed: 24916269]

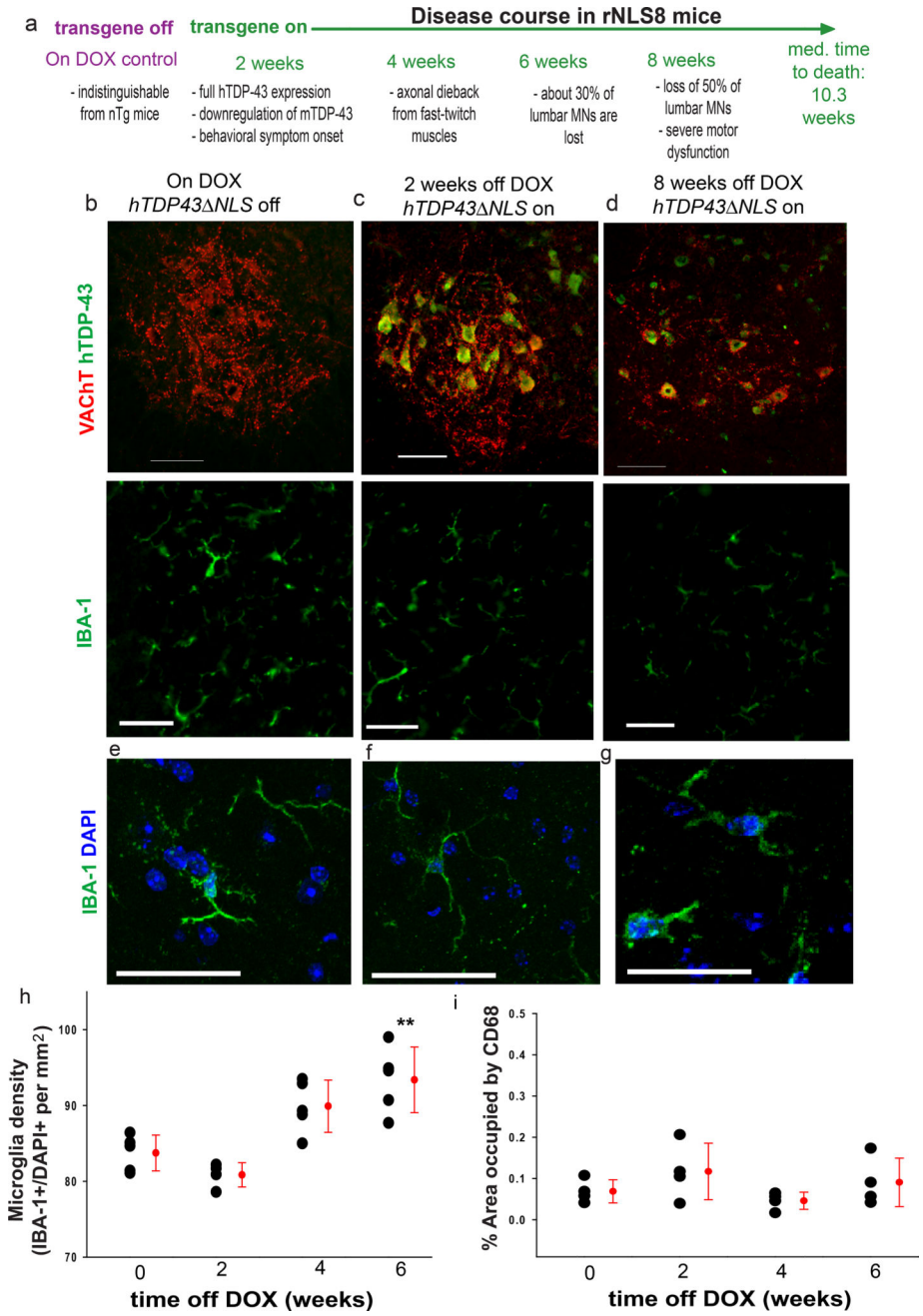

Figure 1. There are only slight changes in microglia density and morphology during disease progression in rNLS8 mouse SC

(**a**) Schematic showing the time course of neuromuscular decline in rNLS8 mice after chronic *hTDP43ΔNLS* expression triggered by DOX removal. (**b–g**) Representative images from lumbar SC of 1 of 5 rNLS8 mice with similar staining, examined at 0, 2, and 8 weeks off DOX. (**b**) Before DOX removal, MNs (VAChT, red) do not express hTDP-43 (red) and microglia have a resting morphology. (**c**) By 2 weeks off DOX, the cytoplasm of MNs express high levels of hTDP-43, yet the microglia remain unreactive. (**d**) At 8 weeks off DOX, microglia appear unreactive, despite widespread nuclear clearance of TDP-43,

aggregated cytoplasmic hTDP-43, and cell death. Scale bar= 100μm. (**e–g**) Cells expressing IBA-1 (green) and DAPI (blue) were analyzed by confocal microscopy, and determined that there were no obvious changes in morphology over the course of disease as assessed in images displayed as a maximum projected z stack of 10 confocal slices. Similar results were observed from 4 independent animals per group. Scale bar= 50 μm. (**h–i**) Only a slight increase in microglia at 6 weeks off DOX (n=5 per group, one way ANOVA, $F_{3,18}$=10.6, p=0.004, **h**) and no change in the activation state are observed, as measured by % area occupied by CD68 throughout the disease course (n=4 mice per group, **i**). Individual data points shown with black circles with group means ± S.D. shown to the right in red.

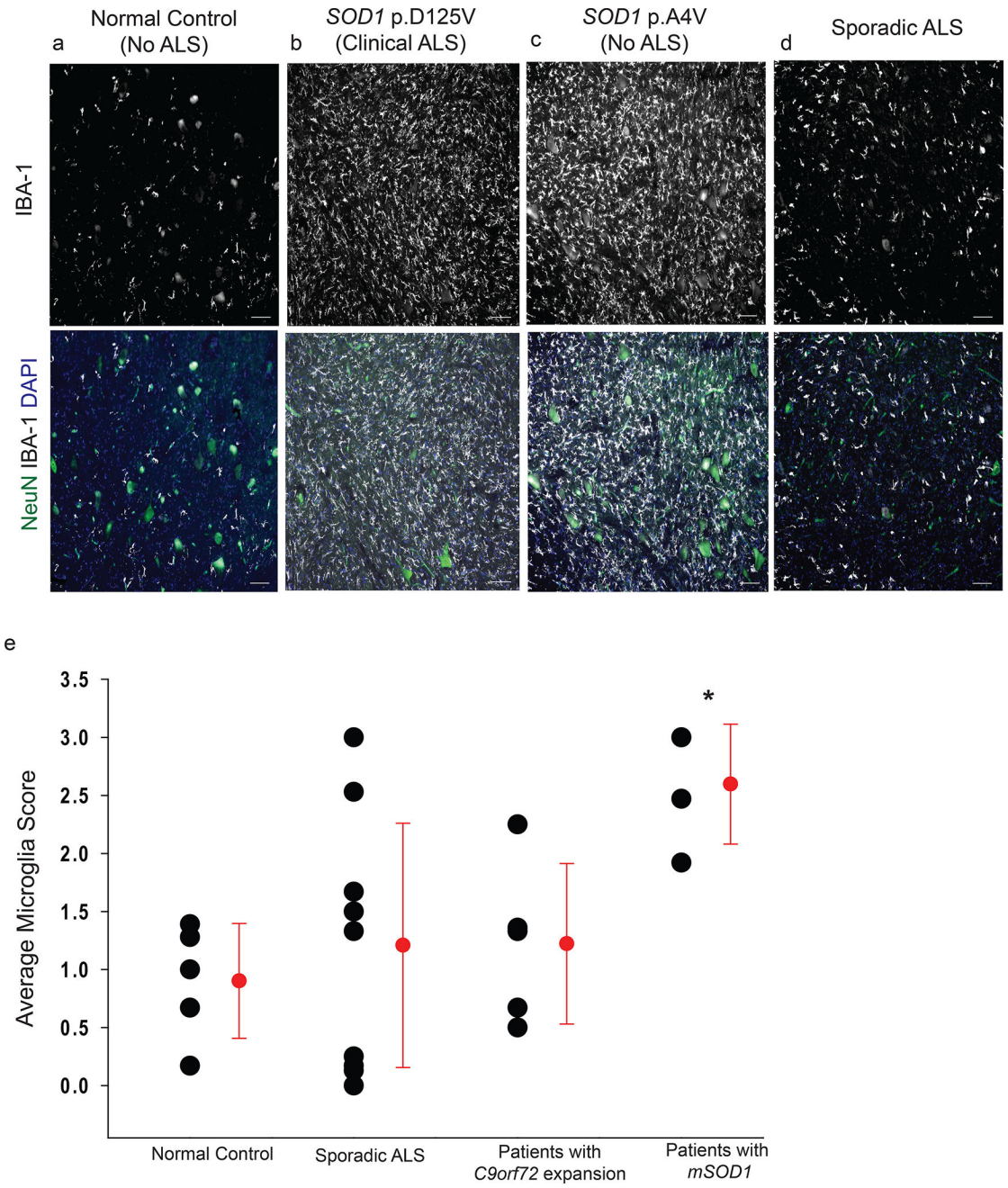

Figure 2. Abundant reactive microglia are found in postmortem samples of lumbar SCs of patients with *SOD1* mutations, but not consistently in samples from sALS or *C9orf72* patients

(**a–d**) Representative images of ventral horn grey matter from 1 of 5 control patients (**a**), a fALS patient with a SOD1 mutation (**b**), a patient with a SOD1 mutation without clinical or pathological evidence of ALS (**c**), and 1 of the 10 patients with sporadic ALS patient (**d**) immunostained with IBA-1 (white) and NeuN (green) show high levels of reactive microgliosis in samples from patients with indicated mutations in *SOD1*, but not in sporadic ALS despite obvious MN loss. Scale bar = 100 μm (**e**) An average of 3 independent scores per patient shows that patients with the *SOD1* mutation, but not sALS patients or those with

a *C9orf72* expansion, have significantly more reactive microglia in ventral horn grey matter than controls, one way ANOVA, $F_{3,24}$=3.8, p=0.03. Individual data points shown with black circles with group means ± S.D. shown to the right in red. See Supplementary Table 1 for patient details.

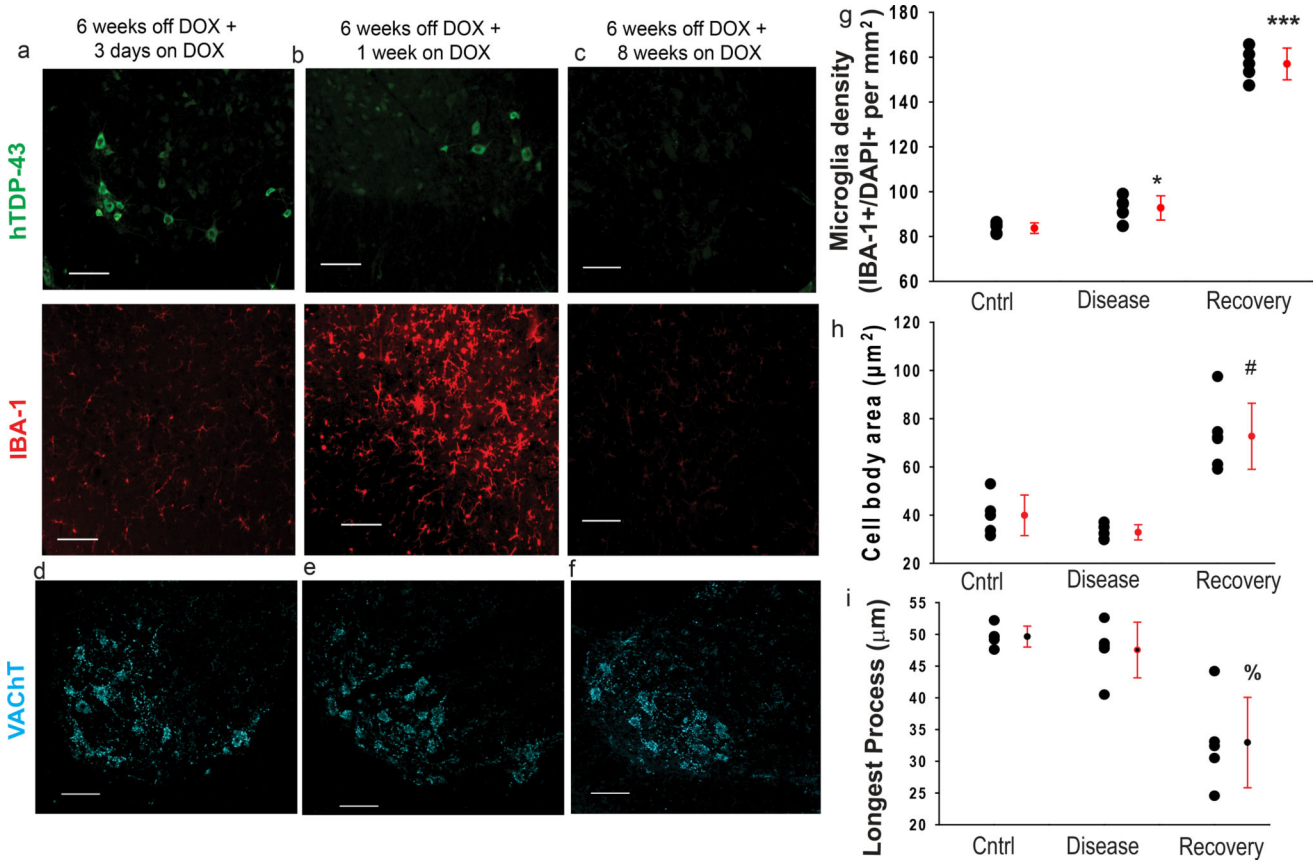

Figure 3. In early disease recovery, there is an abundant increase in the number of microglia and a change in their morphology

(**a–c**) When the transgene is turned off, the hTDP-43 (green) begins to clear from the lumbar SC beginning at 3 days after DOX introduction (**a**), with most clearance happening after 1 week (**b**), and the hTDP-43 being totally cleared from all SC neurons by 8 weeks (**c**). Concurrent with this clearance, there is a dramatic increase in the number of IBA-1^{+} microglia (red), which peaks at 1 week on DOX (**d**) and then returns to baseline levels, despite no change in the number of MNs (**d–f**). After 1 week of transgene suppression, the microglia also have a reactive morphology, with significantly larger cell bodies (**h**) and shorter, thicker processes (**i**).(**g–i**) Individual data points shown with black circles with group means ± S.D. shown to the right in red. Labels “cntrl” are for rNLS8 mice maintained on DOX (n=5), “Disease” are for rNLS mice that were 6 weeks off DOX (n=5), and “Recovery” are rNLS8 mice that were off DOX for 6 weeks and then on DOX for 1 week (n=6). Analyses by one way ANOVA, (**g**) $F_{2,14}$=307.5, *p=0.02, ***p<0.001; (**h**) $F_{2,14}$=26.2, # p<.001; (**i**) $F_{2,14}$=17.1,% p<0.001 . For (**a–f**), similar staining was observed in 6 animals per time-point. Scale bar= 100 µm.

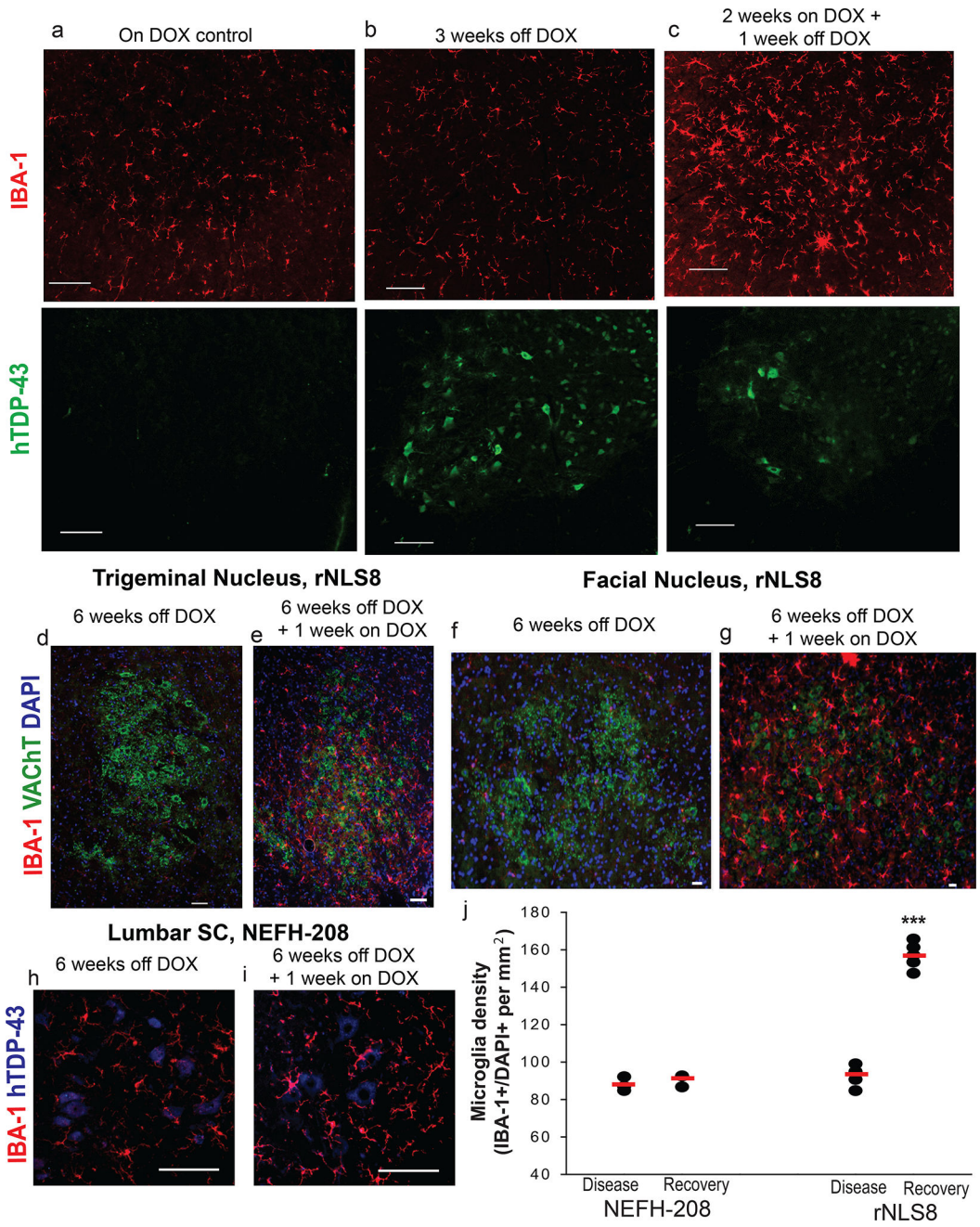

Figure 4. After transgene suppression, microglial activation is independent of prior neuron death

(**a–c**) Representative images of rNLS8 lumbar SC stained with hTDP-43 (green) and IBA-1 (red) shows immunoreactive hTDP43ΔNLS in MNs at the 3 weeks off DOX time-point (**b**), but no change in microglia numbers or morphology. However, when the transgene is suppressed for 1 week, after hTDP-43 expression but prior to MN death (**c**), there is a dramatic increase in reactive microglia. Similar staining was seen in n=6 mice per DOX treatment group. (**d–g**) The same pattern of microglial activation is seen in brainstem nuclei labeled with VAChT (green) and IBA-1 (red), despite no prior cell death of trigeminal MNs (**e**) or facial MNs (**g**). Similar brainstem nuclei staining was seen in 4 rNLS8 mice per DOX

treatment. (**h–j**) Mice with the same inducible system under the same NEFH promoter that express C-terminal fragments of hTDP-43 (amino acids 208–414) do not have the same pattern of microglial activation after neuronal expression (**h**) and 1 week of clearance of hTDP-43 C-terminal fragments (**i**), (designated NEH8-208 Recovery in the dot plot) with mean microglia density for each group indicated with the red line (**j**). NEFH-208, n=3 per group; rNLS8, n=5 per group.***, unpaired, two-tailed t-test, t=−17.6, p= 0.0000002. Scale bars= 100 μm

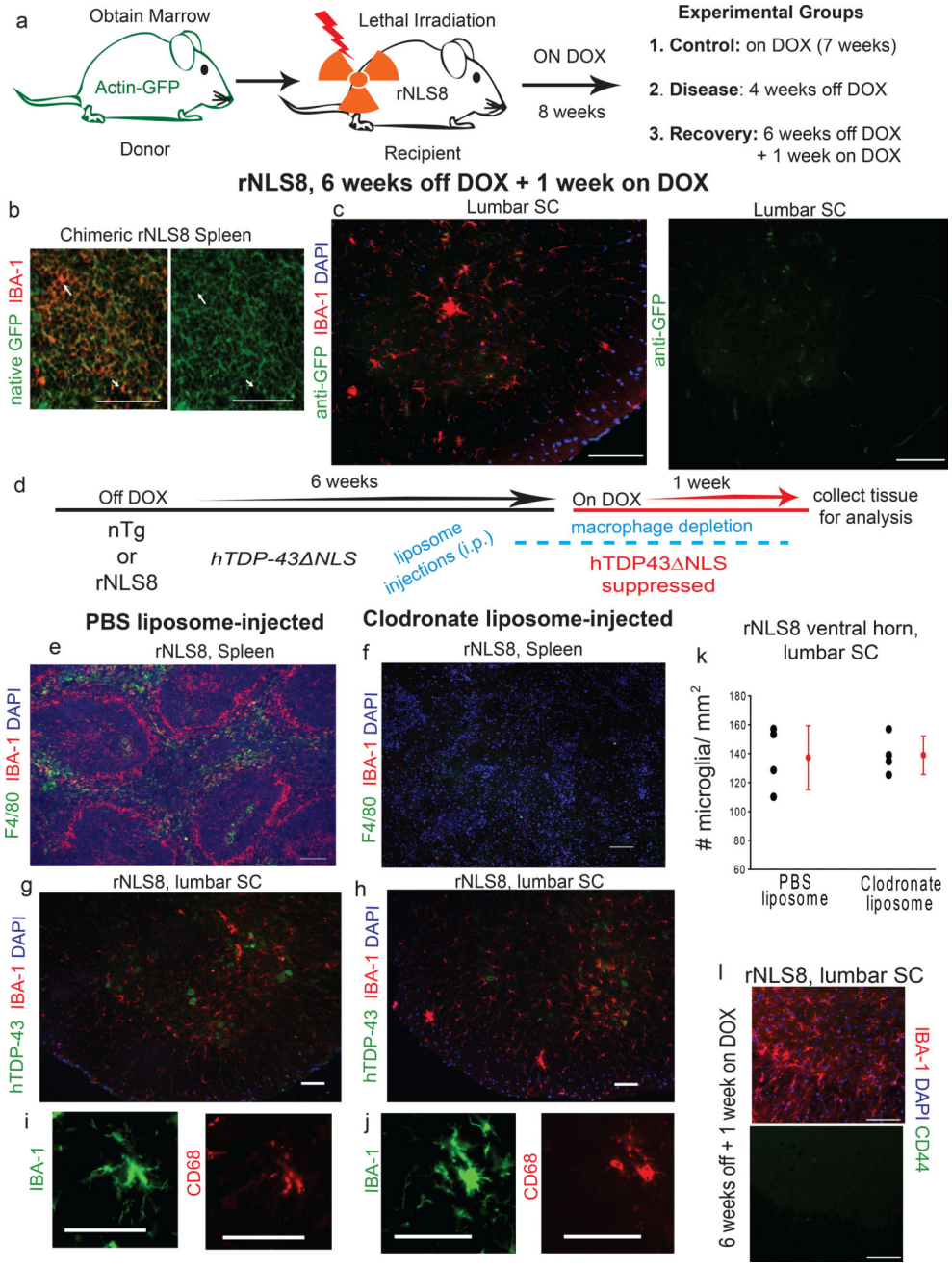

Figure 5. Increased microglia numbers are not the result of infiltrating myeloid cells from the periphery

(**a**) Experimental design: rNLS8 mice are myoablated by irradiation then injected with progenitor cells from Actin-GFP mice. 8 weeks later, animals were either maintained on DOX (n=4), had DOX removed for 4 weeks (n=6), or were 6 weeks off DOX + 1 week on DOX (n=6). (**b**) Representative cryosection of an irradiated rNLS8 mouse spleen stained with IBA-1 (red) shows GFP-positive macrophages, indicating the successful engraftment observed in all 16 mice. (**c**) At 6 weeks off DOX + 1 week on, there was increased reactive microglia in the lumbar SC (IBA-1, red), but these cells GFP (green) negative, a consistent

result in all animals (**d**) Experimental timeline: rNLS8 mice were 6 weeks off DOX + 1 week on, and given injections (i.p.) of either clodronate or PBS-liposomes 10 days prior to analysis. (**e–f**) Representative cryosections of spleen from rNLS8 mice that were injected with PBS-liposomes (**e**) or clodronate-liposomes (**f**) immunostained with F4/80 (green), IBA-1 (red), and DAPI (blue) show intact splenic macrophages after PBS-liposome administration, but ablated populations after clodronate-liposome treatment. (**g–k**) Depleting peripheral myeloid cells had no effect on microgliosis. Individual data points shown with black circles with group means ± S.D. shown to the right in red., n=4. (**l**). Representative cryosection of lumbar SC from 1 of 3 rNLS8 mice during peak microgliosis shows that the microglia are negative for CD44, a marker of peripheral myeloid cells. Scale bars= 100 μm.

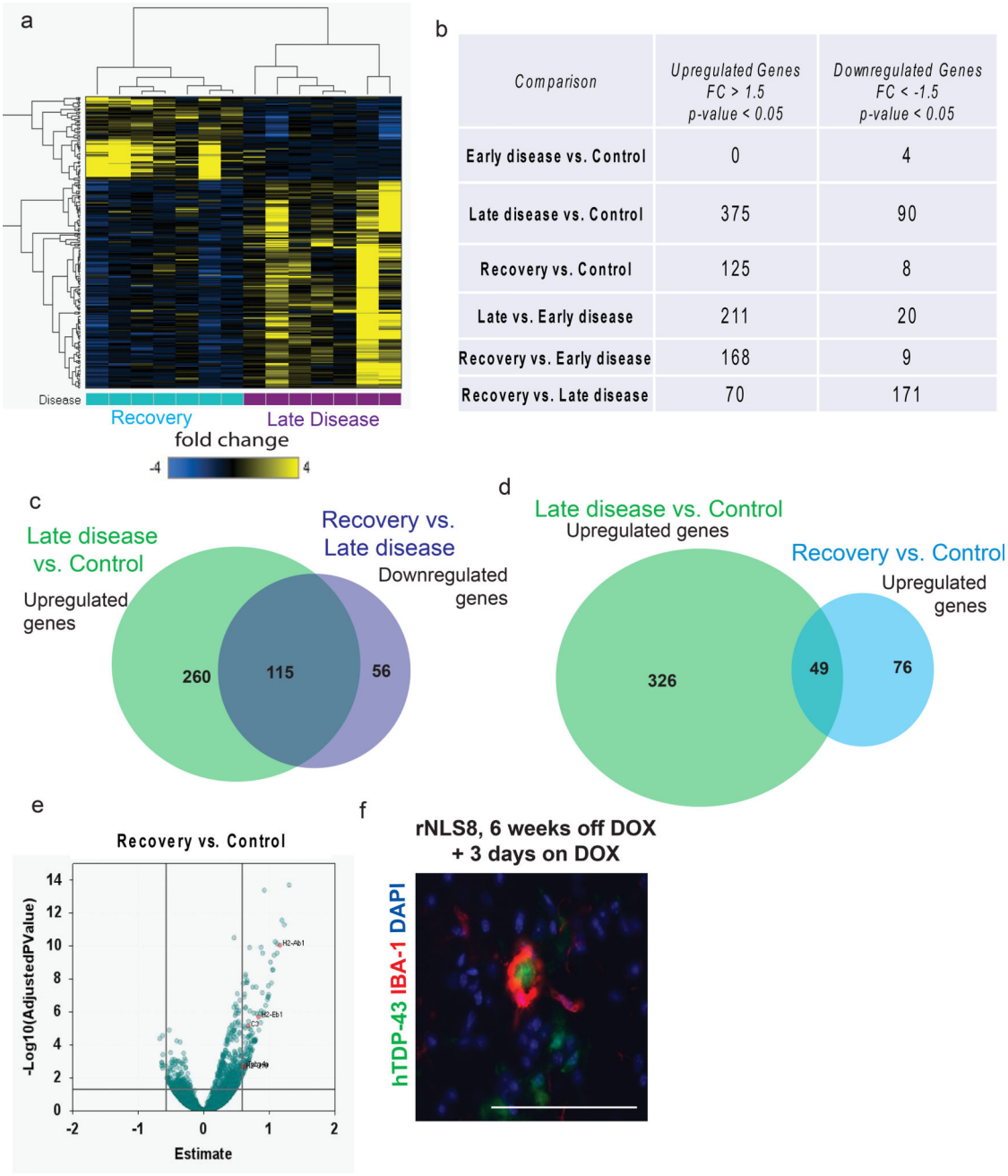

Comparison	Upregulated Genes FC > 1.5 p-value < 0.05	Downregulated Genes FC < -1.5 p-value < 0.05
Early disease vs. Control	0	4
Late disease vs. Control	375	90
Recovery vs. Control	125	8
Late vs. Early disease	211	20
Recovery vs. Early disease	168	9
Recovery vs. Late disease	70	171

Figure 6. Transcriptional profiling of purified SC microglia reveals robust gene changes in microglia during recovery in rNLS8 mice

(**a**) Hierarchical clustering of late disease (purple) and early recovery (blue) samples from SC based on FDR <0.05 and fold change (FC) shows clear separation of gene expression profiles over the course of 1 week of *hTDP43ΔNLS* suppression. Yellow and blue indicate higher and lower expression levels, respectively. (**b**) Table showing the number of differentially expressed genes between indicated SC microglial samples with at least |1.5|FC. Note: There are nearly no gene changes in early disease samples, but robust changes in late disease and early recovery samples. Differential expression was determined using DESeq2, which uses the Wald test for significance testing. “Control”, n=14; “early disease”, n=7;

"late disease", n=9; "recovery", n=9 (**c**) Venn diagram showing numbers of upregulated genes in late disease compared to control (green) and overlap with the downregulated genes between late disease and recovery (purple). (**d**) Venn diagram showing numbers of upregulated genes and overlap between late disease vs. control (green) and recovery vs. control (blue). Note: 76 genes are uniquely upregulated in recovery. (**e**) Volcano plot showing gene expression changes during recovery indicates many upregulated microglia genes and comparatively fewer downregulated genes, FDR <0.05 |FC| 1.5. (**f**) Representative image of microglia (red) and hTDP-43 (green) from 1 of 6 rNLS8 mice at 6 weeks off DOX + 3 days on DOX shows that some neurons are in close contact with reactive microglia. Scale bar = 100 μm.

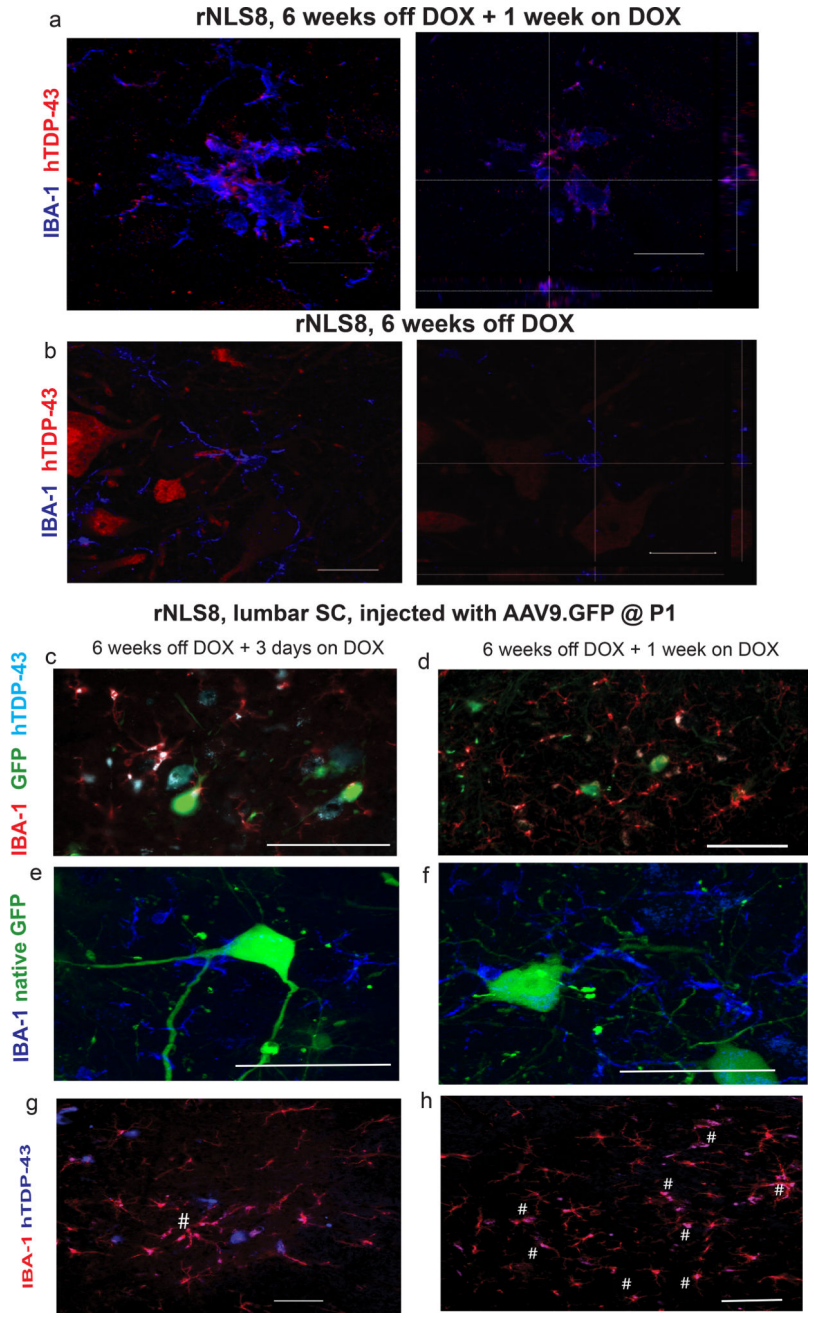

Figure 7. Reactive microglia clear hTDP-43, and this is selective over other neuronally overexpressed cytoplasmic proteins

(**a–b**) Representative images of microglia (blue), and hTDP-43 (red) in an rNLS8 SC after 1 or 0 weeks of hTDP43ΔNLS suppression following 6 weeks of expression, with orthogonal views to show hTDP-43 localization. Scale bar = 25 μm. Similar results were observed in 10 cryosections from n=3 in each group by confocal microscopy. (**c–h**) When AAV9.GFP is overexpressed in MNs of rNLS8 mice, microglia (IBA-1^{+}, red) do not take up GFP (green) after 3 days (**c**) or 7 days (**d**) of recovery, though the majority of microglia do contain the hTDP-43 (blue) by 1 week back on DOX. Scale bar= 100 μm. (**e–f**) Microglia (blue)

surround GFP+ MNs, but do not themselves contain GFP. Scale bar= 50 μm. (**g–h**) Microglia (red) are actively clearing the hTDP-43 (blue) from the rNLS8 SC, and after 1 week back on DOX, the majority of microglia are now positive for hTDP-43 (co-positive cells labeled with #). Representative images shown from 1 of 3 mice at 6 weeks + 3 days, and 4 mice at 6 weeks + 1 week, each with similar results. Scale bar= 100 μm.

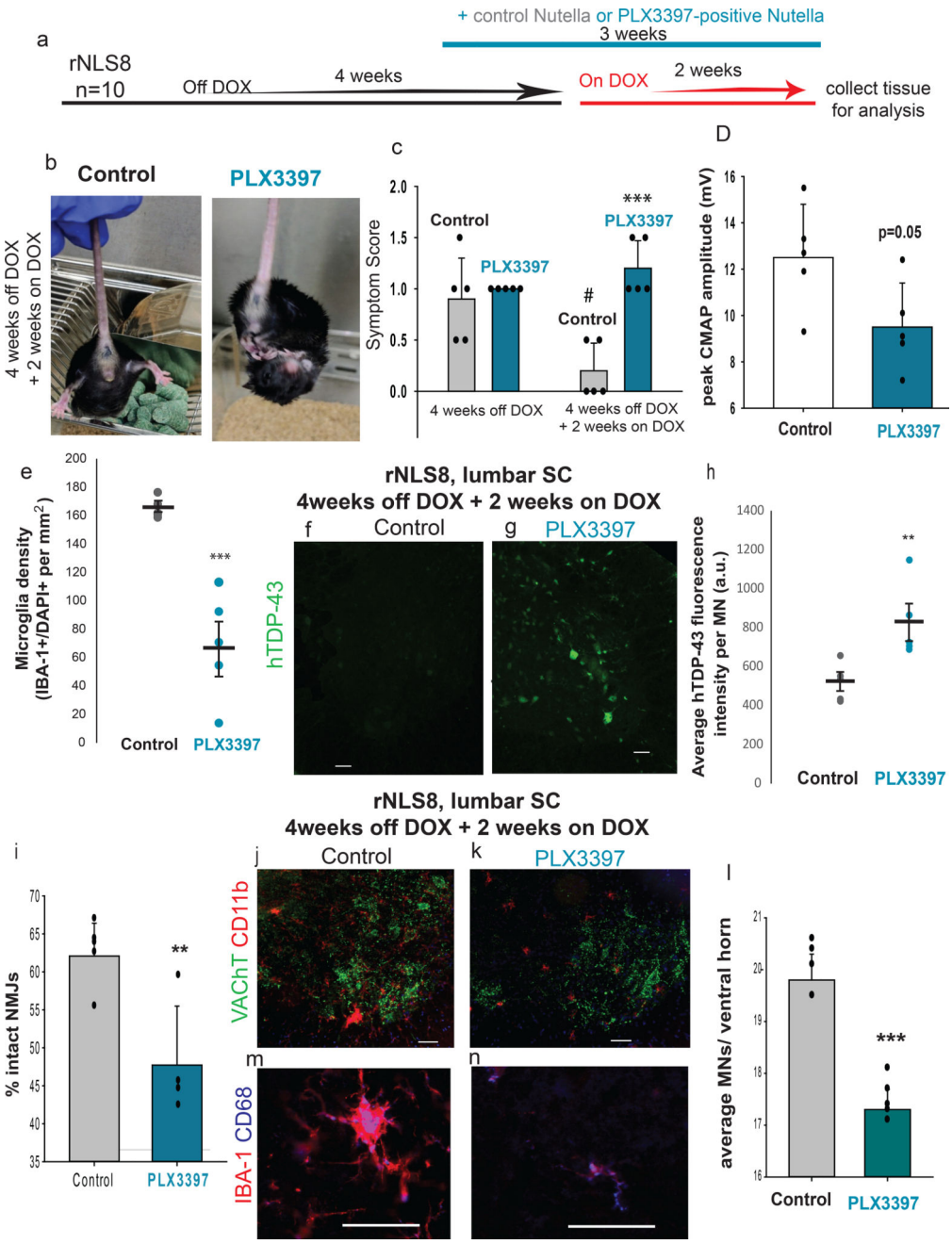

Figure 8. Microglia are necessary for early recovery from MN disease

(**a**) Timeline for experiments using PLX3397 to deplete microglia in rNLS8 mice. (**b–c**) rNLS8 mice given Nutella containing PLX3397 (right), but not control (left) still clasp after 2 weeks on DOX. #, paired t-test, t=3.5, d.f.=4, p=0.02, relative to control mice at 4 weeks off DOX. ***, t=−5.8, d.f.=8, p=0.0004, relative to control mice at 4 weeks off DOX + 2 weeks on. (**d**) PLX3397-treated mice trend towards reduced evoked CMAP. t=2.3, d.f.=8, p=0.05. (**e**) PLX3397 treatment reduced the density of IBA-1^{+} cells in SC. ***, t=5.6, d.f.=8, p=0.0005. (**f–h**) hTDP-43 (green) is cleared from sham-treated rNLS8 MNs (**f**), whereas many hTDP-43-positive MNs remain in the PLX3397-treated lumbar SC (**g**). (**h**)

Quantification of average fluorescence intensity per MN in control (grey) and PLX3397-treated mice (blue) shows that the MNs in microglia-depleted animals are more hTDP-43 immunopositive; **, t=3.3, d.f.= 8, p=0.01. (**i**) PLX3397-treated mice (n=4) have significantly fewer intact NMJs in their TA muscles than controls. **, t=3.5, d.f.=7, p=0.009. (**j–k**) Representative cryosections immunostained with CD11b (red) to label microglia and VAChT (green) to label MNs. (**l**) There are significantly fewer MNs in PLX3397-treated mice compared to control, ***, t=8.7, d.f.=8, p=0.00002. Scale bar= 100 μm. (**m–n**) Many microglia (IBA-1, red) from control (**m**) and PLX3397-treated (**n**) rNLS8 mice express CD68 (blue). Scale bar= 50 μm. Bars represent mean ± S.D., n=5 per group and t-tests unpaired and two-tailed, unless otherwise specified. See Supplementary Table 2 for data summary.